

Guidelines and Parameter Selection for the Simulation of Progressive Delamination

Kyongchan Song

Swales Aerospace/ATK Space, Hampton VA 23669

Carlos G. Dávila, Cheryl A. Rose

NASA Langley Research Center, Hampton VA 23669

Abstract: *Turon's methodology for determining optimal analysis parameters for the simulation of progressive delamination is reviewed. Recommended procedures for determining analysis parameters for efficient delamination growth predictions using the Abaqus/Standard cohesive element and relatively coarse meshes are provided for single and mixed-mode loading. The Abaqus cohesive element, COH3D8, and a user-defined cohesive element are used to develop finite element models of the double cantilever beam specimen, the end-notched flexure specimen, and the mixed-mode bending specimen to simulate progressive delamination growth in Mode I, Mode II, and mixed-mode fracture, respectively. The predicted responses are compared with their analytical solutions. The results show that for single-mode fracture, the predicted responses obtained with the Abaqus cohesive element correlate well with the analytical solutions. For mixed-mode fracture, it was found that the response predicted using COH3D8 elements depends on the damage evolution criterion that is used. The energy-based criterion overpredicts the peak loads and load-deflection response. The results predicted using a tabulated form of the BK criterion correlate well with the analytical solution and with the results predicted with the user-written element.*

Keywords: *Damage, Composites, Progressive Delamination, Virtual Crack Closure Technique (VCCT), Cohesive Elements, Fracture Mechanics.*

1. Introduction

Delaminations in laminated composite structures usually initiate from discontinuities such as matrix cracks and free edges or from embedded defects due to the manufacturing processes. Delaminations can reduce the stiffness and strength of a composite structure. In other cases, delamination can provide stress relief and delay the final failure of the composite structure. Therefore, it is important to analyze the progressive growth of delamination in order to predict the performance of a composite structure and to develop reliable and safe designs.

Abaqus/Standard provides the Virtual Crack Closure Technique (VCCT) and a cohesive element for the simulation of progressive delamination growth. The formulation of the cohesive element is based on the Cohesive Zone Model (CZM) approach for modeling complex fracture mechanisms at the crack tip (Dugdale, 1960 and Barenblatt, 1962). The cohesive zone approach models an extended cohesive zone, or process zone, ahead of the crack-tip using traction-separation laws that relate the opening displacements in the process zone to the resisting tractions. The traction-separation laws are defined in each fracture mode by an initial elastic stiffness, the peak traction, or interfacial strength, and the area under the traction-separation law that is equal to the critical energy release rate.

Fracture simulations using cohesive elements require significant experience for determining the mesh requirements and the selection of properties that characterize the traction-separation response. For typical graphite-epoxy materials, the length of the cohesive zone is less than 1 mm. For an accurate representation of the distribution of tractions ahead of the crack-tip and an accurate simulation of delamination propagation, at least 3 to 5 cohesive elements are required in the cohesive zone. These mesh requirements may not be practical for the simulation of delamination propagation in structural analyses.

Corigliano, 2003, used two-dimensional models of the Double Cantilever Beam specimen (DCB) and identified the pathological dependence of the solution on mesh refinement and attributed the errors in the predictions to the difficulties in calculating the interlaminar stresses accurately. Barua et al, 2007, conducted parametric studies of the effect of interfacial strength and mesh refinement on the predicted load-deflection response. Barua proposed establishing mesh requirements by performing mesh calibration studies using a simple DCB specimen and then applying those calibration results to more complex components made of the same material.

Turon, 2007, proposed a procedure for relaxing the requirement for extremely fine meshes. The procedure consists of increasing artificially the length of the cohesive zone by reducing the interfacial strength. A longer cohesive zone allows for the use of larger elements while maintaining sufficient accuracy in the calculation of the energy release rate.

Turon's procedure for using relatively coarse meshes has been demonstrated with a user-defined cohesive element (UEL) developed by Turon, 2006. In the present paper, Turon's procedure is reviewed and is applied with the Abaqus cohesive element (COH3D8) to provide basic guidelines regarding optimal choices for mesh density and cohesive zone parameters for efficient single- and mixed-mode fracture simulations. Predictions for the load-displacement response for single and mixed-mode fracture specimens obtained using the Abaqus/Standard cohesive element are compared to the analytical solutions.

2. Selection of Constitutive Parameters and Mesh Requirements

The constitutive response of the cohesive elements used in this paper is defined by bi-linear traction-separation law as shown in Figure 1, where T represents the interfacial strength, Δ^c is the critical separation, Δ^{fail} is the separation at failure, and the area under the curve, G_c , is the critical

strain energy release rate. Under mixed-mode fracture, the properties required to define the bilinear traction-separation law are the three critical fracture energies G_{IC} , G_{IIC} , G_{IIIC} , the penalty stiffnesses K_1, K_2, K_3 , and the interfacial strengths T , S_1 , and S_2 . In the present work, the shear strengths in the two orthogonal directions, S_1 and S_2 are assumed to be the same and are referred to as S .

The initial response of the cohesive element is assumed to be linear until a damage initiation criterion is met. The penalty stiffness, K_i , of the bi-linear traction-separation law is defined as

$$K_i = \frac{T_i}{\Delta_i^c} \quad (1)$$

where Δ_i^c is the critical separation for damage initiation. The value of the penalty stiffness must be high enough to prevent interpenetration of the crack faces and to prevent artificial compliance from being introduced into the model by the cohesive elements. However, an overly high value can lead to numerical problems. Several guidelines have been proposed for obtaining the penalty stiffness of a cohesive element. Turon, et al., 2007, proposed an equation for the penalty stiffness for Mode I that ensures that the compliance of the bulk material is much larger than the initial compliance of the cohesive element:

$$K_3 \geq \alpha \cdot \frac{E_3}{t} \quad (2)$$

where α is a parameter much larger than 1, E_3 is the transverse Young's modulus of the material, and t is the thickness of an adjacent sub-laminate. Turon recommends using $\alpha = 50$. This value is used for the penalty stiffness in all of the analyses presented herein. In the present paper, the penalty stiffnesses for all modes are assumed to be the same: $K_1 = K_2 = K_3 = K$.

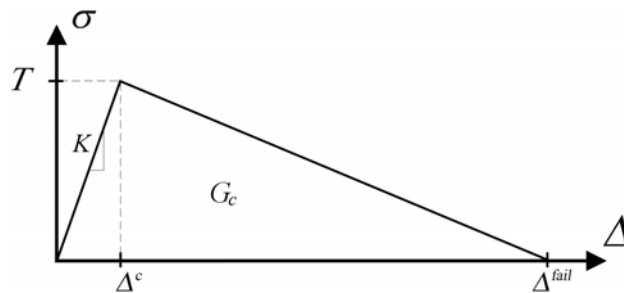


Figure 1. Bilinear traction–separation response of the cohesive element.

To predict the propagation of delamination accurately, it is necessary to have a sufficiently fine finite element discretization of the cohesive zone to ensure a good representation of the interlaminar stress fields. The required maximum size of the cohesive elements can be determined by evaluating the size of the cohesive zone and the number N_e of elements that are needed in the zone.

The length of the cohesive zone, l_{cz} , is the distance from the crack tip to the point when the maximum cohesive traction is attained. Figure 2 describes the length of the cohesive zone. It has been shown that, for infinite-sized geometries, the length of the cohesive zone, l_{cz} , is a material property. For single Mode I and Mode II fracture, the cohesive lengths are approximately (Turon, 2007)

$$l_{cz-I} = ME_2 \frac{G_{IC}}{T^2} \quad \text{and} \quad l_{cz-II} = ME_2 \frac{G_{IIC}}{S^2} \quad (3)$$

where E_2 is the transverse Young's modulus and M is a parameter that depends on the cohesive zone theory used to derive the expression for the cohesive zone length. In this study, Hillerborg's model in which M is equal to 1.0 is used (Hillerborg, 1976). Therefore, the length l_e of the cohesive elements must satisfy the following conditions for Mode I and Mode II:

$$l_e \leq \frac{l_{cz-I}}{N_e} \quad \text{and} \quad l_e \leq \frac{l_{cz-II}}{N_e} \quad (4)$$

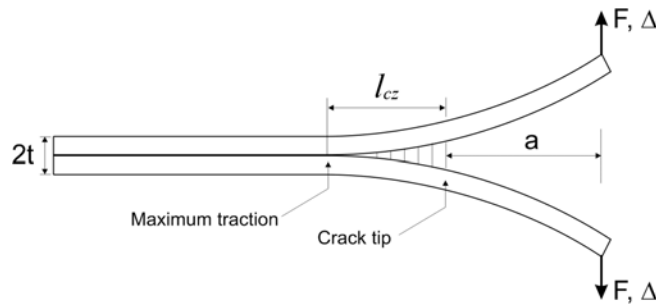


Figure 2. Length of the cohesive zone.

Turon suggests that a minimum of three elements in the cohesive zone is required to accurately represent the fracture energy in the cohesive zone (Turon, 2007). However, the cohesive zone length for typical polymeric composites is less than 1 mm, and such small mesh requirements may render most structural analyses computationally intractable.

When the length of the cohesive zone is negligible compared to the crack length, the propagation of damage is governed by linear elastic fracture mechanics (LEFM) principles that state that the energy release rate for creating a new fracture area must be equal to G_c . Therefore, when LEFM is valid, the effect of the interfacial strengths can be neglected. It can be observed in Equation 3 that the length of the cohesive zone increases as the inverse of the square of the interfacial strength. This suggests that the length of the cohesive zone can be artificially lengthened to ensure that it spans enough elements of a given size. The interfacial normal and shear strengths that are required can be obtained using Equations 3 and 4, which give

$$T^a = \sqrt{\frac{E_2 \cdot G_{IC}}{N_e \cdot l_e}} \quad \text{and} \quad S^a = \sqrt{\frac{E_2 \cdot G_{IIC}}{N_e \cdot l_e}} \quad (5)$$

Therefore, the normal and shear strengths that ensure that enough elements span the cohesive zone are

$$\bar{T} = \text{Min}\{T^a, T\} \quad \text{and} \quad \bar{S} = \text{Min}\{S^a, S\} \quad (6)$$

Abaqus provides four damage initiation criteria: maximum stress, maximum strain, quadratic stress, and quadratic strain criterion. The quadratic stress criterion, shown in Equation 7, is used throughout this paper.

$$\left\{ \frac{\langle \sigma_z \rangle}{\bar{T}} \right\}^2 + \left\{ \frac{\tau_{xz}}{\bar{S}} \right\}^2 + \left\{ \frac{\tau_{yz}}{\bar{S}} \right\}^2 = 1 \quad (7)$$

where the Macaulay bracket, $\langle \rangle$, signifies that the compressive stress does not contribute to damage initiation.

Once the damage initiation criterion of the cohesive element is satisfied, the stiffness of the element is degraded. Equation 8 represents the softening response of the cohesive element

$$\sigma_i = (1 - d)K_i \Delta_i, \quad i = 1, 2, 3 \quad (8)$$

where d is the damage variable, which has the value $d = 0$ when the interface is undamaged, and the value $d = 1$ when the interface is fully fractured.

In the analyses presented herein, we use the energy-based Benzeggagh and Kenane (BK) damage evolution criterion shown in Equation 9 (Benzeggagh and Kenane, 1996)

$$G_C = G_{IC} + (G_{IIC} - G_{Ic}) \left(\frac{G_{Shear}}{G_T} \right)^\eta, \quad (9)$$

where η is the BK material parameter, $G_{Shear} = G_{II} + G_{III}$, and $G_T = G_I + G_{II} + G_{III}$.

In the UEL used herein (Turon, 2006), the BK fracture criterion can be expressed in terms of separations:

$$G_C = G_{IC} + (G_{IIC} - G_{Ic}) \left(\frac{\beta^2}{1 + 2\beta^2 - 2\beta} \right)^\eta \quad (10)$$

where β is the mode mixity ratio defined in terms of separation.

$$\beta = \frac{\Delta_{shear}}{\Delta_{shear} + \langle \Delta_{normal} \rangle} \quad (11)$$

Abaqus provides two methods to implement the BK criterion. In the standard BK option, the fracture toughness G_c given by Equation 9 is determined in terms of the accumulated energy release rates G_{shear} and G_T . This option is specified using the following command lines

```
*DAMAGE EVOLUTION, TYPE=ENERGY,
MIXED MODE BEHAVIOR=BK, POWER= $\eta$ 
```

Alternatively, the BK criterion can also be specified with G_c supplied in tabular form. Using Equation 10, a table of G_c can be specified as a function of the mode mixity ratio. This option is specified using the following command lines

```
*DAMAGE EVOLUTION, TYPE=ENERGY,
MIXED MODE BEHAVIOR=Tabular
 $G_c$ ,  $\phi_i$ 
```

where ϕ_i is defined as

$$\phi_i = \frac{2}{\pi} \tan^{-1}(\beta / (1 - \beta)) \quad (12)$$

In the following simulations, both options are used and their corresponding results are compared to the results obtained with a user-defined element and with analytical solutions.

3. Analyses of progressive delamination growth

The Abaqus cohesive element COH3D8 and the user-defined cohesive element COH_UEL developed by Turon, 2006 were used to develop finite element (FE) models of the double cantilever beam (DCB) specimen and the end-notched flexure (ENF) specimen to simulate progressive delamination growth under Mode I and Mode II fracture, respectively. In Sections 3.1 and 3.2, the results of nonlinear analyses performed to investigate the effect of mesh density and interfacial strength on the predicted load-deflection response of the DCB and ENF specimens are presented. From the progressive delamination growth predictions of the FE models for single-mode fracture, the mesh density required for solution convergence and the corresponding normal and shear strengths for a given material are obtained. Progressive delamination growth predictions of single-mode fracture obtained with the Abaqus cohesive element and COH_UEL correlate closely with each other. Therefore, only the progressive delamination growth predictions obtained with the Abaqus cohesive element are presented with the analytical solutions.

FE models of the mixed-mode bending (MMB) specimen were developed using the mesh density and the interfacial strengths that resulted in converged results for the single-mode analyses. In Section 3.3, the predicted progressive delamination results for the MMB specimen with the Abaqus cohesive element and the COH_UEL are compared with analytical solutions and with Abaqus VCCT predictions.

FE models of each specimen are developed using the material properties of AS4/3501-6 that are provided in Table 1. All specimens are unidirectional and the fibers are aligned with the direction of fracture propagation.

Table 1. Mechanical and interface material properties of AS4/3501-6.

| | | | | | | |
|------------------------|------------------------|------------------------|------------|-----------|----------|----------|
| E_1 | E_2 | E_3 | ν_{12} | G_{12} | G_{13} | G_{23} |
| 148 GPa | 10.50 GPa | 10.50 GPa | 0.27 | 5.61 GPa | 5.61 GPa | 3.17 GPa |
| G_{IC} | G_{IIc} | G_{IIIc} | T | S | η | |
| 0.08 kJ/m ² | 0.55 kJ/m ² | 0.55 kJ/m ² | 53.78 MPa | 86.88 MPa | 1.8 | |

3.1 Double Cantilever Beam Specimen

FE models of a DCB specimen are developed to investigate the influence of mesh refinement and the normal interfacial strength on the predicted responses for Mode I simulation. The length of the specimen, L , is 101.6 mm long, and the width is 7.62 mm. The specimen is composed of two sub-laminates of thickness $t=1.524$ mm. The initial crack length, a_0 , is 29.21 mm. Each sub-laminate has a stacking sequence of $[0_3]$. The configuration of the specimen is shown in Figure 3.

The DCB specimen is modeled with two layers of 4-node shell elements S4 that are connected together with cohesive elements. The reference surfaces of the sub-laminates are moved from the mid-surface of the sub-laminates to the contact surface between the two sub-laminates using the shell property option `OFFSET`

Three levels of mesh refinement were considered and the corresponding models are labeled DCB-1, -2, and -3. All three models have a uniform mesh in a 10 mm-long damage propagation zone ahead of the crack tip, which is labeled c_0 in Figure 3. The element sizes in zone c_0 of models DCB-1, DCB-2, and DCB-3 are 1.0 mm, 0.5 mm, and 0.32 mm, respectively.

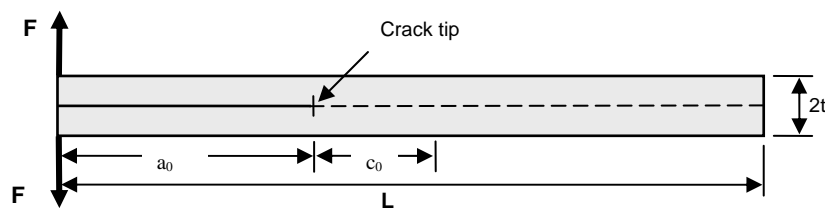


Figure 3. Configuration of double cantilever beam (DCB) specimen.

The cohesive zone length for Mode I fracture calculated from Equation 3 is $l_{cz_I}=0.29$ mm. The penalty stiffness determined from Equation 2 with $\alpha=50$ is $K=344$ GPa/mm. The nominal normal strength provided in Table 1 and the adjusted normal strength obtained using Equation 5 are used to study the influence of mesh size and normal strength on the prediction of fracture propagation

in Mode I. Three different values for the number of elements within the cohesive zone, N_e , are substituted into Equation 5 to calculate the adjusted normal strength. The number of elements within the cohesive zone and the adjusted normal strength corresponding to the different mesh refinements, DCB-1, -2, and -3, are shown in Table 2.

Table 2. Adjusted normal strengths corresponding to the three mesh refinements.

| Number of Elements in Cohesive Zone | DCB-1 $l_{e, Model} = 1\text{ mm}$ | DCB-2 $l_{e, model} = 0.5\text{ mm}$ | DCB-3 $l_{e, model} = 0.32\text{ mm}$ |
|-------------------------------------|---------------------------------------|---|--|
| $N_e = 1$ | 29.6 MPa | 41.9 MPa | 53.8 MPa |
| $N_e = 3$ | 17.1 MPa | 24.2 MPa | 30.2 MPa |
| $N_e = 5$ | 13.2 MPa | 18.7 MPa | 23.4 MPa |

The predicted load-deflection responses obtained using model DCB-1 are compared to the analytical solution (Reeder, 2004) in Figure 4. The model with the nominal normal strength and an adjusted normal strength with $N_e = 1$ significantly overpredicts the strength of the DCB specimen and the response does not follow the softening response of the analytical solution. The responses predicted using an adjusted strength with $N_e = 3$ and 5 compare well with the analytical solution. However, these models exhibit over-softening before the peak load and they display spurious oscillations during delamination propagation. Therefore, model DCB-1 is too coarse to predict accurately the propagation of delamination, even when the strengths are lowered using Equation 5.

The predicted load-deflection responses obtained using model DCB-2 are shown in Figure 5. The response predicted with the nominal normal strength and the response predicted with an adjusted normal strength with $N_e = 1$ significantly overpredict the peak load. Both responses exhibit minor oscillations during fracture propagation. The responses and the peak loads obtained with $N_e = 3$ and $N_e = 5$ correlate well with the analytical solution.

The load-deflection responses obtained using the most refined model, DCB-3, are shown in Figure 6. For this level of mesh refinement, the adjusted strength with $N_e = 1$ is approximately equal to the nominal strength. The solution obtained with nominal strength overpredicts the peak load and the softening response of the analytical solution by approximately 7%. The peak loads and the load-deflection responses predicted using normal strengths adjusted with $N_e = 3$ and $N_e = 5$ correlate well with the analytical solution.

A comparison of the results obtained with models DCB-1, DCB-2, and DCB-3 indicates that, when used in conjunction with an adjusted strength with $N_e = 3$, model DCB-2 is the coarsest model that provides accurate results.

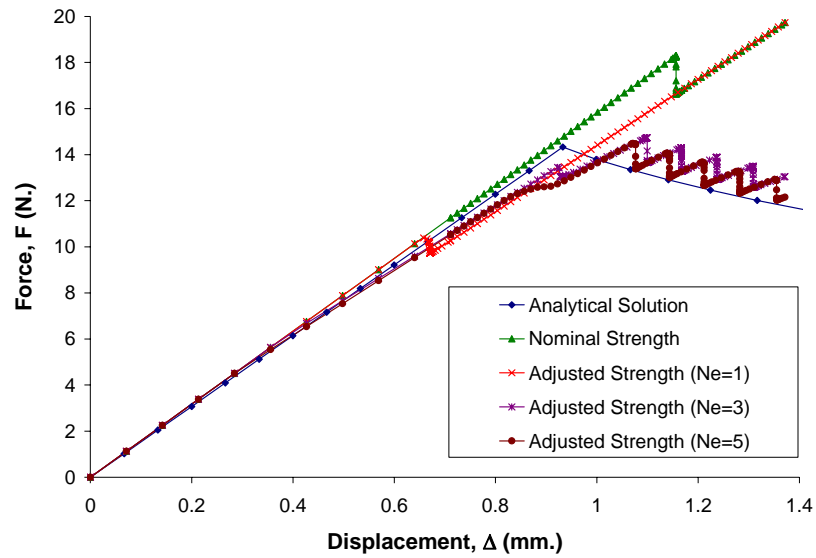


Figure 4. Effect of the normal interfacial strength on the predicted load-deflection response for FE model DCB-1.

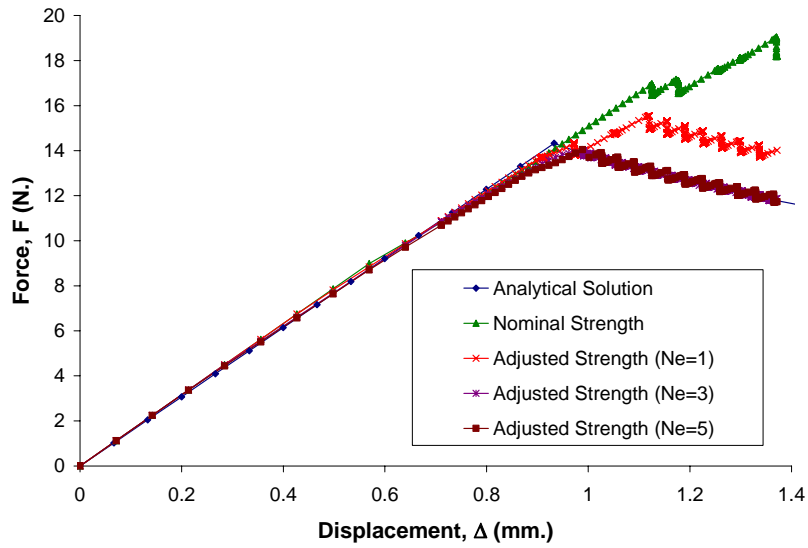


Figure 5. Effect of the normal interfacial strength on the predicted load-deflection response for FE model DCB-2.

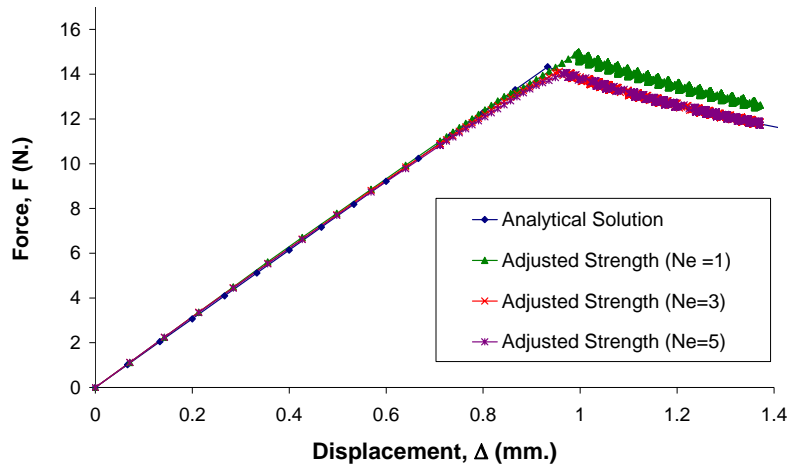


Figure 6. Effect of the normal interfacial strength on the predicted load-deflection response for FE model DCB-3.

3.2 End Notched Flexure (ENF) Specimen

FE models of the ENF specimen were developed to investigate the influence of mesh refinement and the interfacial strength on the predicted response for Mode II fracture simulation. The ENF specimen has the same dimensions and stacking sequence as the DCB specimen analyzed in Section 3.1. For the ENF specimen, the force, F , is applied at the middle of the specimen. The ENF specimen configuration and the boundary conditions are shown in Figure 7.

FE models of the ENF specimens with two levels of mesh refinement, indicated as model ENF-1 and ENF-2, are developed to investigate the sensitivity of the predicted responses to the mesh refinement. These models have a uniform mesh in a damage propagation zone of length c_0 equal to 21.6 mm ahead of the crack tip. The span-wise element length in zone c_0 of Models ENF-1 and ENF-2 is 1.0 mm and 0.5 mm, respectively. The cohesive zone length for Mode II fracture calculated from Equation 3 is $l_{cz_II} = 0.77$ mm.

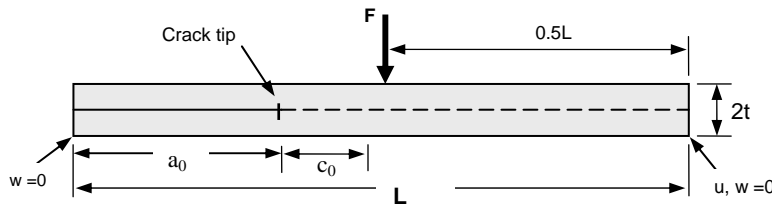


Figure 7. Configuration and boundary conditions of the End Notched Flexure specimen.

A comparison of the predicted load-deflection responses of the FE models and the analytical solution (Mi, 1998) is shown in Figure 8. The results of the FE models for the ENF specimen are consistent with the analytical solutions and indicate that both models are sufficiently refined and that the difference in element size between the two models has a minimal influence on the predicted responses. In addition, when using an element size of 1 mm or smaller, no adjustment to the nominal shear strength is necessary. These results indicate that the simulation of progressive delamination of a composite structure subjected to Mode II I does not require a mesh as fine as a mesh required for Mode I fracture.

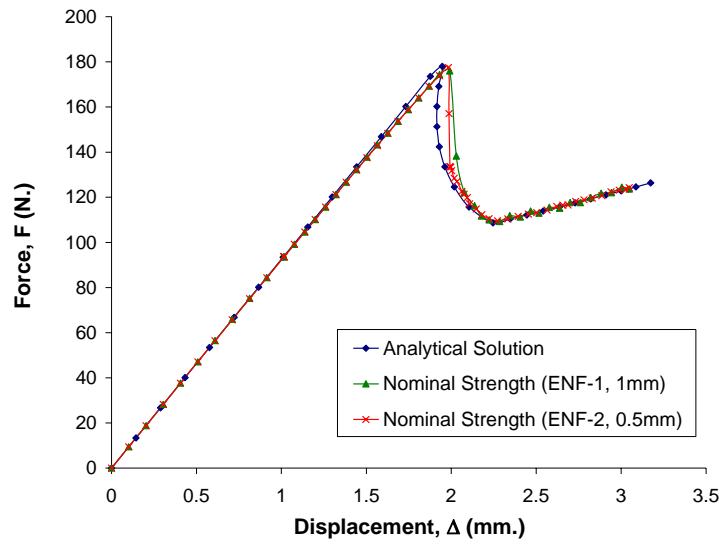


Figure 8. Effect of mesh refinement on the predicted load-deflection response of ENF FE models.

3.3 Mixed-Mode Bending (MMB) Specimen

The Abaqus cohesive element and the COH_UEL are used to develop FE models of the MMB specimen. The specimen is 100 mm-long and 25.5 mm-wide with two 2.3 mm-thick sub-laminates. The initial crack length, a_0 , is 27 mm. The experimental set-up of Reeder, et al., 1990, shown in Figure 9 is modeled. The level of mode mixity in the MMB is applied by varying the length of the applied load lever arm, d , of the test apparatus.

In the FE simulation of the MMB specimen, the lever arm length, d , is equal to 52.8 mm and the corresponding mixed-mode ratio, G_{II}/G_T , is equal to 0.2. The penalty stiffness determined from Equation 2 with $\alpha=50$ and $t=2.3$ mm is equal to $K=228\text{GPa/mm}$.

The FE model of the MMB specimen has a uniform mesh in a damage propagation zone ahead of the crack tip of length c_0 equal to 23.0 mm. The element size in the propagation zone was selected to be $l_e = 0.5$ mm, and the number of elements in the cohesive zone is chosen as $N_e=3$. These values were found to provide converged results in the analyses of the DCB and ENF specimens described in the previous sections. Models of the MMB were created with the Abaqus cohesive elements and with user-defined elements. Two damage evolution options were evaluated with the Abaqus cohesive elements: the standard BK and the tabular options described in Section 2. To improve the convergence rate, a viscoelastic regularization factor of 10^{-4} was used in the analyses for both the Abaqus cohesive element and the user-defined element.

Using Equation 5, the reduction factor of the normal strength, \bar{T}/T , is 45 %. The ENF analyses indicate that the nominal shear strength of the material does not need to be reduced. However, to investigate the influence of the shear strength on the mixed-mode fracture predictions, three different shear strengths are used: the nominal shear strength, S , the shear strength adjusted by using Equation 5, \bar{S} , and the shear strength reduced by the same reduction factor as the normal strength, \tilde{S} . The adjusted normal and shear strengths are reported in Table 3.

Table 3. The shear strengths of the cohesive element.

| | AS4/3501-6 |
|--|------------|
| \bar{T} : Adjusted Normal Strength by Equation 5 | 24.2 MPa |
| S : Nominal Shear Strength | 86.9 MPa |
| \bar{S} : Shear Strength Adjusted by Equation 5 | 63.7 MPa |
| \tilde{S} : Shear Strength Adjusted by Mode I reduction factor | 39.2 MPa |

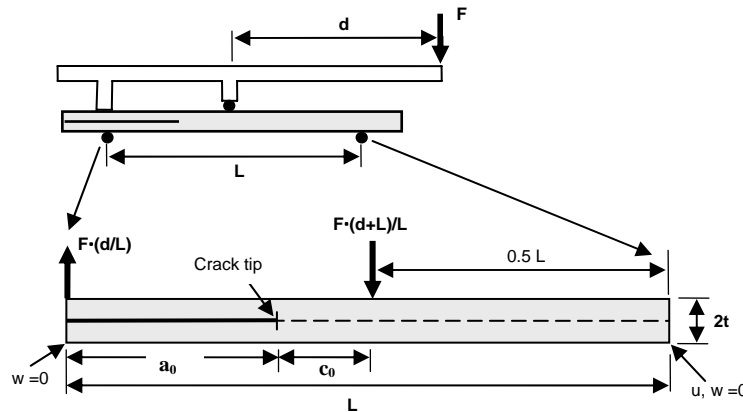


Figure 9. Configuration, experimental set-up, and boundary conditions of the MMB specimen.

The predicted load-deflection responses obtained using Abaqus cohesive elements, the VCCT tool, and the analytical solution are shown in Figure 10. The VCCT response and the analytical

solution correlate well with each other. The responses predicted with the standard BK option and the Abaqus COH3D8 elements overpredict the force required for crack propagation by approximately 35%. However, when the tabulated form of the BK option is used, the predicted results correlate well with the analytical solution and with the VCCT prediction. The predicted solutions are also sensitive to the normal-to-shear strengths used in the analyses. For the ratios used, the three load-deflection curves obtained with the tabulated BK option differ by approximately 6%.

The results predicted with the standard BK option and with the tabulated BK option should be identical to each other if the mode-mixity does not change during damage evolution. The fact that the results shown in Figure 10 do not correlate well with each other indicates that the mode-mixity changes during damage evolution. This unexpected result will require further investigation of the evolution of damage in the MMB test.

The predicted load-deflection responses obtained using the user-defined cohesive element (Turon, 2006), COH_UEL, are shown in Figure 11. When the adjusted normal and nominal shear strengths, \bar{T} , S , are used, the FE model overpredicts the peak load and the load-deflection response compared to the analytical solution and the VCCT prediction. The results also indicate that reducing the shear strength influences the predicted load-deflection response of the FE model. When the adjusted normal and shear strengths, \bar{T} , \bar{S} , obtained by Equation 5 are used for the interfacial strengths, the predicted load-deflection responses obtained with the COH_UEL correlate well with the analytical solution and with Abaqus VCCT predictions. Although the nominal shear strength can be used as shear strength of COH_UEL for single Mode II fracture, the predicted response of FE models with COH_UEL indicates that both normal and shear strengths needed to be adjusted using Turon's guideline to obtain accurate fracture simulations for the mixed-mode fracture.

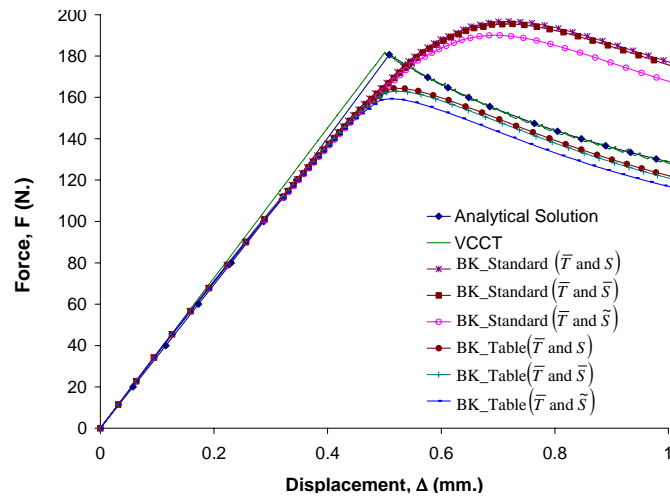


Figure 10. Load-deflection response of MMB specimen with Abaqus COH3D8 cohesive element.

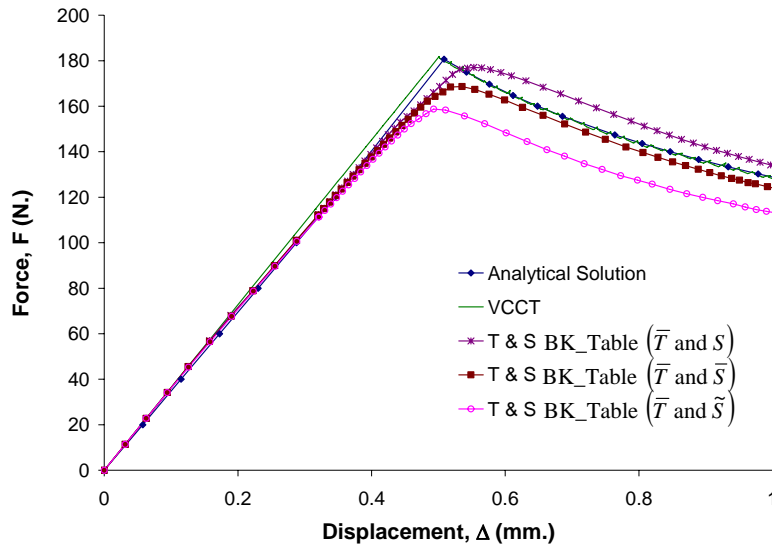


Figure 11. Load-deflection response of MMB specimen with user-defined COH_UEL cohesive element.

4. Concluding Remarks

Turon's methodology for selecting analysis parameters for the simulation of delamination propagation using relatively coarse meshes is reviewed and used to determine analysis parameters for use with the Abaqus/Standard cohesive element. The Abaqus cohesive element, COH3D8, and a user-defined cohesive element are used to model a DCB specimen, an ENF specimen, and a MMB specimen to simulate progressive delamination in Mode I, Mode II, and mixed-mode fracture, respectively. For single-mode fracture, the predicted responses obtained with the Abaqus cohesive elements correlate well with the analytical solutions when the interfacial normal and shear strengths are determined using Turon's methodology. For mixed-mode fracture, the predicted response obtained with Abaqus cohesive element depends on the damage evolution criterion selected. The results using the standard BK overpredict the analytical results by as much as 35%, but when the BK criterion is supplied in tabulated form, the results correlate well with the VCCT results and with the analytical solution.

The selection of cohesive element parameters and mesh requirements for fracture propagation in structural subcomponents should be established by performing single-mode fracture simulations in simple specimens of the same material. In the present paper, the optimal mesh density and analysis parameters for the simulation of fracture of a mixed-mode bending test were determined from parametric simulations of DCB and ENF specimens. This procedure should also be applied for the simulation of fracture in more complex structures.

5. References

1. Barenblatt, G., "The Mathematical Theory of Equilibrium Cracks in Brittle Fracture," *Advances in Applied Mechanics*, Vol. 7, pp. 55-129, 1962.
2. Barua, A., and Bose, K., "On the Optimum Choices of Cohesive-Zone Parameters Describing Initiation and Propagation of Cracks," in *ECCOMAS Thematic Conference on Mechanical Response of Composites*, Ed. P. P. Camanho et al., Porto, Portugal 2007.
3. Benzeggagh, M. L. and Kenane, M., "Measurement of Mixed-mode Delamination Fracture Toughness of Unidirectional Glass/epoxy Composites with Mixed-mode Bending Apparatus," *Compos. Sci. Technol.*, Vol. 56, No. 4, pp. 439-449, 1996.
4. Corigliano, A., Milne, I., Ritchie, R. O., and Karihaloo, B., "Damage and Fracture Mechanics Techniques for Composite Structures," *Comprehensive Structural Integrity*, Pergamon, Oxford, 2003, pp. 459-539.
5. Dugdale, D. S., "Yielding of Steel Sheets Containing Slits," *Journal of the Mechanics and Physics of Solids*, Vol. 8, pp. 100-104, 1960.
6. Hillerborg, A., Modéer, M., and Petersson, P. E., "Analysis of Crack Formation and Crack Growth in Concrete by Means of Fracture Mechanics and Finite Elements," *Cement and Concrete Research*, Vol. 6, No. 6, pp. 773-781, 1976.
7. Mi, Y., Crisfield M. A., Davis G. A. O., Hellweg, H. B. "Progressive Delamination Using Interface Elements," *J Composites*, Vol. 32, pp. 1246-72, 1998.
8. Reeder, J.R., Demarco, K., and Whitley, K. S., "The Use of Doubler Reinforcement in Delamination Toughness Testing," *Composites Part A: Applied Science and Manufacturing*, Vol. 35, No. 11, pp. 1337-1344, 2004.
9. Reeder, J. R., and Crews Jr., J. R. "Mixed-Mode Bending Method for Delamination Testing," *AIAA Journal*, Vol. 28, No. 7, pp. 1270-1276, 1990.
10. Turon, A. Camanho, P. P., and Dávila, C. G., "A Damage Model for the Simulation of Delamination in Advanced Composites under Variable-Mode Loading," *Mechanics of Materials*, Vol. 38, No. 11, pp.1072-1089, 2006.
11. Turon, A., Dávila, C. G., Camanho, P. P., and Costa, J., "An Engineering Solution for Mesh Size Effects in the Simulation of Delamination Using Cohesive Zone Models," *Engineering Fracture Mechanics*, Vol. 74, No. 10, pp. 1665-1682, 2007.